applied sciences

MDPI

Article

Nanofiltration of Simulated Acid Mine Drainage: Effect of pH and Membrane Charge

Ye Wee Siew [1], Karina Listiarini Zedda [2] and Svetlozar Velizarov [1,*]

[1] LAQV-Requimte, DQ, FCT, Universidade NOVA de Lisboa, 2829-516 Caparica, Portugal; siewyewee@gmail.com

[2] R&D Membranes, BU Liquid Purification Technologies, LANXESS-IAB Ionenaustauscher GmbH, D-06731 Bitterfeld-Wolfen, Germany; karina.zedda@lanxess.com

* Correspondence: s.velizarov@fct.unl.pt; Tel.: +351-212948314; Fax: +351-212948550

Received: 30 November 2019; Accepted: 3 January 2020; Published: 5 January 2020

Abstract: Acid mine drainage (AMD) is a severe form of environmental pollution that has the potential to contaminate surface and ground waters by introducing heavy metals and lowering the pH. The feasibility of using nanofiltration (NF) as a potentially attractive and cost-effective remediation method to treat acid mine drainage was investigated in this study. The performance of an acid-stable NF membrane focusing on the effects of the water pH and membrane charge on ion rejection was systematically studied. A single salt solution experiment showed that Mg, Cu, and Mn containing species were highly rejected at above 97%. Below the membrane iso-electric point (IEP), Mn showed an increased rejection of 99%, while Mg and Mn rejections were relatively constant within the investigated pH range of pH 2 to 7. Rejection of monovalent Cl^- decreased with increasing concentration of an accompanying divalent SO_4^{2-}, showing that Donnan related effects are more prominent at higher ionic concentrations. The sulfate rejection decreased drastically below pH 3 due to the formation of HSO_4^-, which permeated through the membrane, which can be utilized as a way of separation of the metals from the accompanying sulfur-containing compounds. For mixed salt solutions, rejection of silicate dropped from 52% to 38% when magnesium sulfate was added, owing to shielding of the membrane surface charge by Mg^{2+} ions. The NF process performance with a simulated AMD solution was found to be similar to that with model salt solution experiments, both in terms of ion rejection values and general pH-dependent rejection trends. The results obtained can be used as a fast preliminary tool for evaluating the feasibility of using NF for treating AMD with a given ionic composition and pH.

Keywords: acid mine drainage; nanofiltration; ion rejection; Donnan effect

1. Introduction

Acid mine drainage (AMD) is an acidic, sulfur-rich, metallic wastewater, originating from mine discharge of both operational and abandoned mines [1]. During mining operations, sulfide minerals such as pyrite (FeS_2), mackinawite (FeNiS), and chalcocite (Cu_2S) are being exposed. These exposed minerals are oxidized by the combined effect of water and oxygen resulting in the release of metal and sulfates. For example, AMD can be formed from pyrite through a series of oxidative reactions (Equations (1)–(4)) where ferric iron acts as the primary oxidant [2,3]:

$$2FeS_{2\,(s)} + 7O_{2\,(g)} + 2H_2O_{\,(l)} \rightarrow 2Fe^{2+}{}_{(aq)} + 4SO_4{}^{2-}{}_{(aq)} + 4H^+{}_{(aq)}, \quad (1)$$

$$4Fe^{2+}{}_{(aq)} + O_{2\,(g)} + 4H^+{}_{(aq)} \rightarrow 4Fe^{3+}{}_{(aq)} + 2H_2O_{\,(l)}, \quad (2)$$

$$Fe^{3+}{}_{(aq)} + 3H_2O_{\,(l)} \rightarrow Fe(OH)_{3\,(s)} + 2H^+{}_{(aq)}, \quad (3)$$

$$FeS_{2\,(s)} + 14Fe^{3+}{}_{(aq)} + 8H_2O_{(l)} \rightarrow 15Fe^{2+}{}_{(aq)} + 2SO_4{}^{2-}{}_{(aq)} + 16H^{+}{}_{(aq)}. \quad (4)$$

Typically, AMD is characterized by high acidity (pH 2 to 4), high sulfate concentration (1000 to 20,000 mg/L) and elevated concentration of metal mixtures which may include iron, manganese, copper, calcium, lead, magnesium, sodium, and nickel [4,5]. When left untreated, AMD can contaminate soils and water sources (ground and surface) by introducing heavy metals and lowering pH, thus pollution by AMD endangers the well-being of humans, animals, plants, and the ecology as a whole. AMD composition can vary in pH and ionic composition, depending on the mine location and mineral rock types. As a result of these diverse conditions, the choice of treatment is dictated by both economic and environmental factors.

For the selection of AMD treatment, Johnson and Hallberg [3] suggested three guidelines. Firstly, decision-makers have to be wary of the hidden economic and environmental costs associated with each treatment. For example, the cost of fossil fuels for transportation of materials and the price of waste disposal are usually overlooked. Secondly, it is important to ensure the sustainability of the chosen remediation method. Ideally, the end products of mine water treatment should be viewed as a potential resource rather than waste and valorized, accordingly. Sales of recovered and recycled resources could be used to fund the cost of treatment. Lastly, legislation and regulation from the relevant environmental authorities is the overriding factor that determines the choice of the treatment system. The disposal and wastewater discharge criteria usually demand near complete removal of sulfate, metals, and acidity from the AMD.

So far, lime neutralization and biological treatment have been used as conventional treatment approaches to AMD. However, alternative methods such as ion exchange and membrane separation have the advantage to recover metal and acid in addition to AMD mitigation, as an effort to achieve zero liquid discharge [6].

Lime ($Ca(OH)_2$) or limestone ($CaCO_3$) are added to AMD to precipitate sulfate as gypsum and metals as hydroxides. The gypsum sludge is then removed by gravity separation, which raises the pH [7]. Massive amounts of gypsum sludge with no economic value are generated and have to be disposed of in large land areas. Moreover, this process is expensive, labor-intensive, and unable to meet the discharge criteria in some instances [8].

Biological treatment systems can be classified based on either active systems (bioreactors) or passive systems (aerobic and anaerobic wetlands) [3]. In general, biological systems rely on the ability of sulfate-reducing bacteria found in carbon sources (e.g., manure, wood chips) to generate alkalinity in AMD and remove metals. Sulfate is reduced to sulfide to form metal precipitates. Concurrently, hydrogen sulfide generated by the bacteria raises the wastewater pH [8,9].

Separation by ion exchange (IEX) technology is based on selective binding and elution interaction between the ions and appropriate IEX resins. It is a simple technology, which is efficient in removing trace impurities, and especially suitable if large volumes of dilute ionic solutions are to be treated. It is possible to remove copper (II) using a chelating ion exchanger under acidic conditions [10]. Recovery of copper, nickel, and cobalt from AMD using IEX has been proven successful by Nodwell and Kraotvil [11]. IEX becomes less attractive if concentrated AMD is to be treated because of the need for more frequent IEX resin regeneration.

Membrane technology is an attractive alternative to conventional AMD treatment options. Both reverse osmosis (RO) and nanofiltration (NF) are well-established methods for water desalination. They are highly efficient, cost-effective, and easy to scale-up processes. In the face of an ever-increasing stringent environmental criteria, applications of RO and NF are gaining acceptance from the mining industry. It is considered that NF offers a good opportunity compared to conventional methods to treat AMD, such as the preferential passage of mono-charged ions (e.g., hydrogen sulfate, protons) allowing for further recovery of sulphuric acid and high rejection of multi-charged ions, such as transition metals and rare earth elements [12]. NF is preferred over RO when treating metal pollutants as it provides a higher permeate flux at a lower pressure while yielding acceptable rejection performance [13]. This leads to reduced capital investment, and lower system operating and maintenance costs. Moreover,

NF can be used to concentrate and recover target metals from AMD, which can be exploited as an invaluable resource commodity [12,14].

Mullet et al. [14] investigated the impact of feed pH and membrane charge on NF performance for AMD treatment for two NF membranes (NF 270 and TS 80). They concluded that the retention of metal cations was maximized when the feed solution pH was below the membrane isoelectric point (IEP). In another study, the performance of three commercial membranes (NF99, DK, GE) at different pressures and concentrations on treating a Chilean copper mine AMD sample was investigated [8]. All membranes tested showed a promising high rejection of heavy metals (>98%). It can be concluded that membrane performance for single and mixed salt solutions can provide a clue to the performance of NF treating AMD streams.

Effect of Feed Solution pH

An NF membrane exhibits an amphoteric behavior and the membrane charge varies according to the feed solution pH that it is exposed to. This was demonstrated in a pioneering study by Hagmeyer and Gimbel [15], in which the zeta potential of Desal 5 DK membrane was expressed as a function of the solution pH. The isoelectric point (IEP) of the membrane corresponds to the intersection of the curve with the *x*-axis where the zeta potential or net membrane charge is zero. This usually corresponds to the minimum rejection, where size exclusion is the only active separation mechanism [16]. Below the IEP, a positive zeta potential is observed indicating a positive membrane surface charge and vice versa for pH >IEP.

Based on this behavior, the separation performance in terms of permeate flux and solute rejection can be altered. Mänttäri et al. [17] showed that commercial polyamide thin film composite (TFC) membranes exhibit a more open polymeric structure (resulting in higher permeate flux and lower solutes rejection) under alkaline conditions. However, an opposite observation was made by Tang et al. [18] with the permeation of sodium chloride solution using a polyester composite NF membrane. This study found that the electrostatic repulsion between the (–COO–) groups on the membrane surface and the OH^- groups in the feed solution at high pH results in pore shrinkage which consequently decreases the permeate flux. A higher flux was also observed at low pH due to the conversion of amino groups to RH_3N^+, which increases the overall hydrophilicity of the membrane and enlarged its pores [19] due to a reduced electrostatic repulsion brought about by the decreased H^+ concentration in the feed solution. This discrepancy in reported findings shows that the effect of pH on the separation performance depends largely on the membrane chemistry.

The objective of the present study was to investigate the relationship between ions rejection, feed pH and membrane charge by characterizing the performance of a commercial NF membrane for single salt and mixed salt solutions at different pH values. These salts contain ions found in a typical AMD solution. Subsequently, ion rejection performance for a model AMD at different pH values was systematically investigated and characterized.

2. Materials and Methods

2.1. Materials and Apparatus

An in-house made NF membrane (referred to as Membrane A) was used in this study. It is a thin film composite, which consists of a PAN (polyacrylonitrile) substrate support layer and a surface skin layer, which chemical composition is under know-how protection. This surface skin layer is cross-linked on top of the PAN substrate. The membrane pure water permeability at 25.0 °C was determined to be 1.99 L/(m^2.h.bar). The membrane rejection of glucose (3% in RO water) at 40 bar is 96%.

All salts were weighed using a weighing balance (Mettler Toledo XS6002S) and added directly to deionized (DI) water (with approximately 2.0 µS/cm of conductivity and pH 5.8) to make up a target salt solution. $MgSO_4{\cdot}7H_2O$, $CaSO_4{\cdot}2H_2O$, and $NaSiO_3$ were obtained from Sigma Aldrich.

$CuSO_4 \cdot 5H_2O$, $Mn(NO_3)_2 \cdot 5H_2O$, HCl, and NaOH were obtained from Merck. NaCl, Na_2SO_4, $NaNO_3$, and $C_6H_{12}O_6$ were obtained from Applichem. Single and mixed salt solution feed compositions, as well as the pH range investigated in this study, are shown in Tables 1 and 2, respectively.

Table 1. Single salt solution feed compositions.

Salt	Concentration	pH
$MgSO_4$	4000 ± 100 mg/L $MgSO_4$	2.0–7.0 ± 0.1
$CuSO_4$	100 ± 10 mg/L Cu	2.0–5.4 ± 0.1
$Mn(NO_3)_2$	165 ± 5 mg/L Mn	2.0–5.1 ± 0.1

Table 2. Mixed salt solution feed compositions.

Salt	Concentration	pH
$NaSO_4$ and NaCl	2000 ± 200 mg/L Na_2SO_4 and 700 ± 50 mg/L NaCl	2.0–7.0 ± 0.1
$NaSO_4$ and NaCl	0.001 ± 0.0001 mol/L Na_2SO_4 and 0.001 ± 0.0005 mol/L NaCl 0.005 ± 0.0002 mol/L Na_2SO_4 and 0.005 ± 0.0017 mol/L NaCl 0.010 ± 0.0013 mol/L Na_2SO_4 and 0.010 ± 0.003 mol/L NaCl 0.015 ± 0.0004 mol/L Na_2SO_4 and 0.015 ± 0.0037 mol/L NaCl	7.0 ± 0.1
Na_2SiO_3 and $MgSO_4$	15 ± 1 mg/L Si and 2000 mg/L $MgSO_4$	7.0 ± 0.1

New membrane coupons were used in each set of experiments. Prior to the start and after the end of each experiment set, permeation tests were performed at standard test conditions (2000 mg/L $MgSO_4$ T = 25.0 °C, ΔP = 10 bar and a feed flow rate = 4.0 L/min). Permeate flux and ion rejection results were compared between the start and after the end of the standard condition experiments run for 30 min, so as to ensure that the membrane integrity remained intact throughout a given experiment set. For all experiments, the feed operating pressures were fixed at 10 bar. The feed solution pH values were adjusted to the targeted pH (±0.1) using either 10% (v/v) HCl or 10% (v/v) NaOH.

2.2. Model AMD Solution Design

The model AMD solution used in this study was designed as an average of the compositions of different mine waters as detailed in Table 3 with reference to 6 mine water solutions. They included 3 real mine water (MW) solutions (MW A: Australian Copper MW, Chilean Copper MW, and Brazilian Uranium MW) and 3 model compositions (MW B, MW C, and MW D) recreated from MW A by Mullett et al. [14]. The final target ion concentration was calculated from the salts used in single salt and mixed salt experiments. Table 4 shows the model AMD solution feed composition investigated in this study. Na_2SiO_3 was omitted from the model AMD solution composition as it causes other salts in the solution to precipitate. Mn and Cu were chosen as the representative heavy metal ions in the model AMD solution.

Table 3. Composition of mine water (MW) samples from other works and target composition for model acid mine drainage (AMD).

Compound	Mullett et al. [14]				Al Zoubi et al. [8]		Target
	Australian MW (mg/L)	MW B (mg/L)	MW C (mg/L)	MW D (mg/L)	Chilean Copper MW (mg/L)	Brazilian Uranium MW (mg/L)	Model AMD (mg/L)
pH	4.56	5.50	4.10	2.60	<2.50	NA	2.0–5.0
Calcium, Ca^{2+}	480	260	280	270	325.9	89.9	270
Copper, Cu	410	410	610	590	2298	NA	390
Magnesium, Mg^{2+}	770	870	900	900	630.6	8.84	2300
Manganese, Mn	440	420	530	500	224.5	115	500
Sodium, Na^{+}	2000	3000	3800	3600	6.89	1.7	3600
Sulfate, SO_4^{2-}	6900	8700	10,500	10,200	14,337	1508	10,327
Chloride, Cl^{-}	2300	2300	3000	2900	NA	0.21	5559
Nitrate, NO_3^{-}	NA	NA	NA	NA	NA	NA	1129

NA—Not available.

Table 4. Model AMD solution feed composition used in the present study.

Ion	Concentration (mg/L)	pH
Calcium, Ca^{2+}	250 ± 10	2.0–5.0 ± 0.1
Copper, Cu	370 ± 10	
Magnesium, Mg^{2+}	2400 ± 100	
Manganese, Mn	490 ± 10	
Sodium, Na^{+}	3200 ± 100	
Sulfate, SO_4^{2-}	8700 ± 200	
Chloride, Cl^{-}	5000 ± 200	
Nitrate, NO_3^{-}	930 ± 50	

2.3. Membrane Filtration Experiments

NF experiments were performed using an in-house custom-built flat sheet cross-flow filtration membrane coupon tester (CT) (Figure 1), capable of testing 6 membrane coupons concurrently.

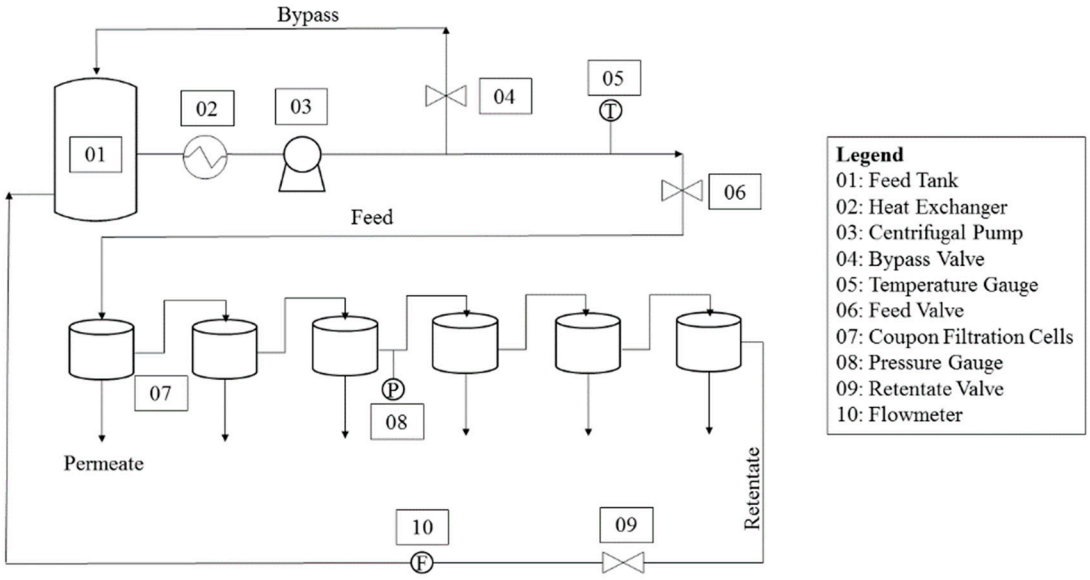

Figure 1. Cross flow nanofiltration setup.

The CT consisted of 6 membrane coupon filtration cells arranged in a series configuration (feed originates from the retentate of the upstream adjacent cell), each with a membrane area of 26.55 cm^2. The installation consists also of a 60 L feed tank and a high-pressure centrifugal pump.

Nanofiltration experiments were carried out in a batch recirculation mode (total permeate recovery of about 0.1%). By efficient cell design and appropriate hydrodynamic conditions, the effect of concentration polarization (see Figures A1 and A2 in Appendix A) was rendered negligible during all filtration experiments. As such, the ion rejection and permeate flux were calculated using the following Equations:

$$R_{app} = \left(1 - \frac{c_P}{c_f}\right), \tag{5}$$

$$\Pi = iMRT, \tag{6}$$

$$\Delta\Pi = \Pi_f - \Pi_p, \tag{7}$$

$$J_v = A(\Delta P - \Delta\Pi) = \frac{V_p}{A_m t}, \tag{8}$$

in which the symbols and subscripts have their common meanings as specified in Appendix B.

The target salts were added into the feed tank and recirculated to ensure their complete dissolving and homogenous mixing within the system. Feed sampling was performed before the start of each experiment and, if necessary, adjusted accordingly to the targeted concentrations. The salt concentrations throughout the system were assumed to be constant since the volume loss by permeate sampling (approximately 6 × 50 mL) was negligible compared to the feed volume (60 L).

The feed recirculation flow rate was measured by a flow meter after the last filtration cell. Three valves were used to adjust the fluid flow to the desirable operating conditions. The pressure was measured using a pressure gauge at the retentate of the third filtration cell. This pressure was regarded as the imposed operating pressure, ΔP, as the pressure drop across the 6 membrane coupon filtration cells was insignificant (below 0.05 bar). Lastly, the temperature was maintained at 25 °C using a heat exchanger.

All filtration experiments were first run at 10 bar for 1 h for membrane compaction. After that, permeate samples were collected. The sampling time for all the experiments was 30 min.

3. Analytical methods

3.1. Conductivity—Concentration Calibration Curve

Calibration curves were constructed to establish a relationship between the concentration of magnesium sulfate (10–100 mg/L and 1000–4500 mg/L) and conductivity from pH 3 to 7. Magnesium sulfate salt was weighed using a weighing balance (Mettler Toledo XS6002S and XP504) and added to 1 L of deionized water. The pH, conductivity, and temperature were noted using a multimeter (Schott Prolab 4000) after the salt had completely dissolved. Next, the pH was raised to pH 7 using 10% NaOH from an initial pH of 5.6–5.8. Similarly, the pH and conductivity were noted, after which the pH was lowered stepwise (interval of 1) to pH 3 to obtain the corresponding conductivity. Magnesium sulfate concentration (mg/L) was expressed as a function of conductivity (μS/cm) at pH 3, pH 4, and pH 5 to 7, respectively. Calibration of sodium chloride solution at pH 7 was performed in a similar manner as for the magnesium sulfate solution.

3.2. Spectrophotometer

A VIS spectrophotometer (Hach Lange DR3900) capable of measuring wavelength between 320 to 1100 nm was used in this study. The following Hach LCK cuvette tests were used: LCK 153 and 353 (for sulfate), LCK 329 (for copper), LCK 427 (for calcium and magnesium), LCK 339 (for nitrate), LCW 028 (for silicon), and LCW (for manganese). When necessary, samples were diluted to meet the required concentration range before measurement. Interferences in the cuvettes due to the presence of other ionic species were verified according to the specification. The test concentrations were adjusted accordingly during the design of the experiment set to prevent such errors.

3.3. Argentometric Titration

Chloride ion measurements were performed using argentometric titration. Each sample was titrated against a solution of known silver nitrate concentration. Chloride ions react with silver (Ag I) to form insoluble silver chloride. A blood-red color is formed at the titration end-point.

3.4. Ion Chromatography (IC)

Ion chromatography was used to measure the concentration of anions in the synthetic AMD experiments. The anions bound to the anion exchange resins in the chromatographic column were subsequently eluted based on their charge and size.

3.5. Inductively Coupled Plasma-Optical Emission Spectroscopy (ICP-OES)

ICP-OES was used to measure the concentration of cations in the synthetic AMD experiments. The samples were injected into an argon plasma and excited at high temperatures. The atomic emission

emanating from the plasma was collected with a lens and imaged in the silt of a wavelength selection device, where the concentration of the cations was determined.

3.6. Electrokinetic Characterization

Streaming potential measurements of the membrane surface were performed using a SurPASS system (Anton Paar, Graz, Austria) with adjustable gap cell 0.001M KCl salt solution and Ag/AgCl electrodes, as described in previous studies [20–22].

4. Results and Discussion

4.1. Streaming Potential Data

In this study, the streaming potential measurements were conducted between pH values of 3 to 10. As can be seen in Figure 2, the isoelectric point (IEP) of the membrane in a KCl solution was found to be at a pH of 4.7 below which the surface becomes positively charged.

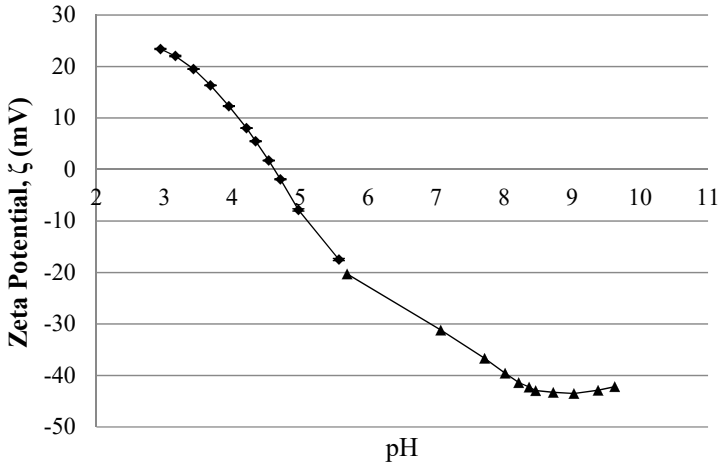

Figure 2. Graph of zeta potential of Membrane A as a function of pH.

Specific adsorption SO_4^{2-} anions could be expected to shift the IEP to a lower pH value. In any case, at pH 7, for which all standard rejection experiments using magnesium sulfate were performed, Membrane A is negatively charged. At this pH value, rejection of sulfate is greater than the chloride due to stronger electrostatic repulsion (higher valency of SO_4^{2-} vs. Cl^-), thus resulting in the Donnan effect, namely preferential rejection of divalent to monovalent ions of the same charge [23]. Passage of Cl^- ions is more prominent at higher salt concentrations due to the screening effect brought about by increasing Na^+ concentration. The presence of Na^+ shields the negative charge on the membrane surface causing a decreased Cl^- rejection. Due to the higher valency and larger size of sulfate, sulfate rejection remained high for all tested concentrations (see Section 4.2).

4.2. NF Performance in Single Salt Solutions

To assess the membrane performance with minimal interferences, single salt experiments with selected compounds were performed, namely magnesium sulfate, copper sulfate, and manganese nitrate. In addition, sulfate rejection was determined separately. Figure 3a shows the magnesium rejection and permeate flux as a function of feed pH.

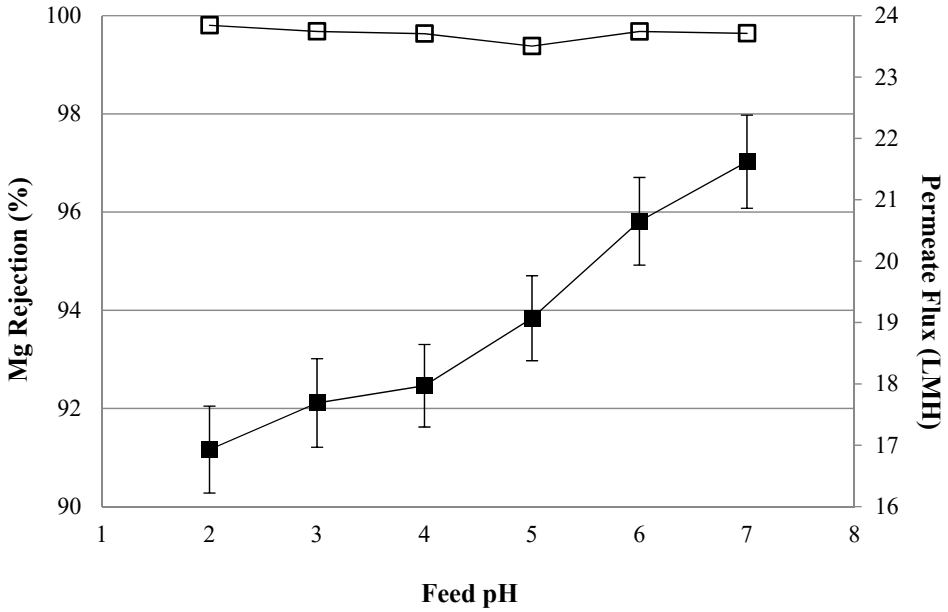

(**a**)

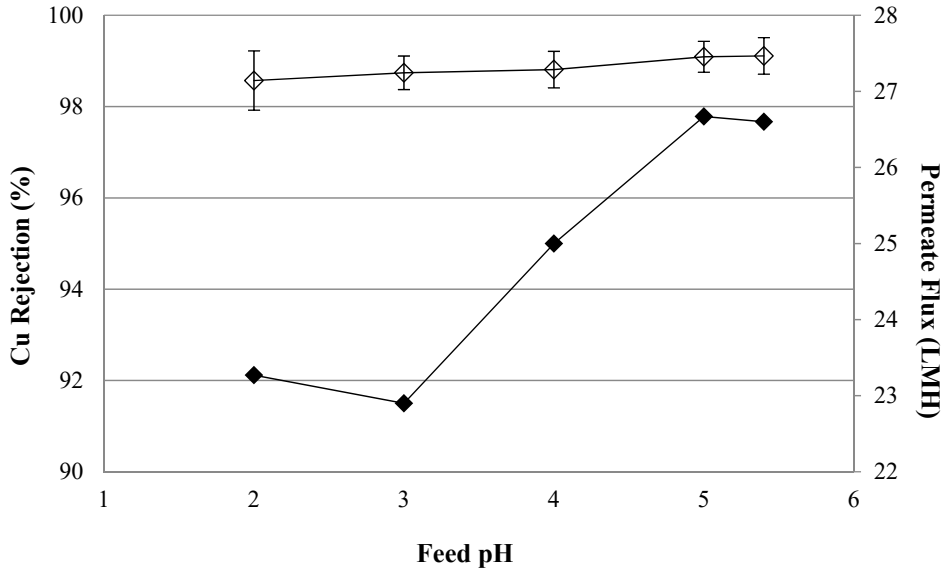

(**b**)

Figure 3. *Cont*.

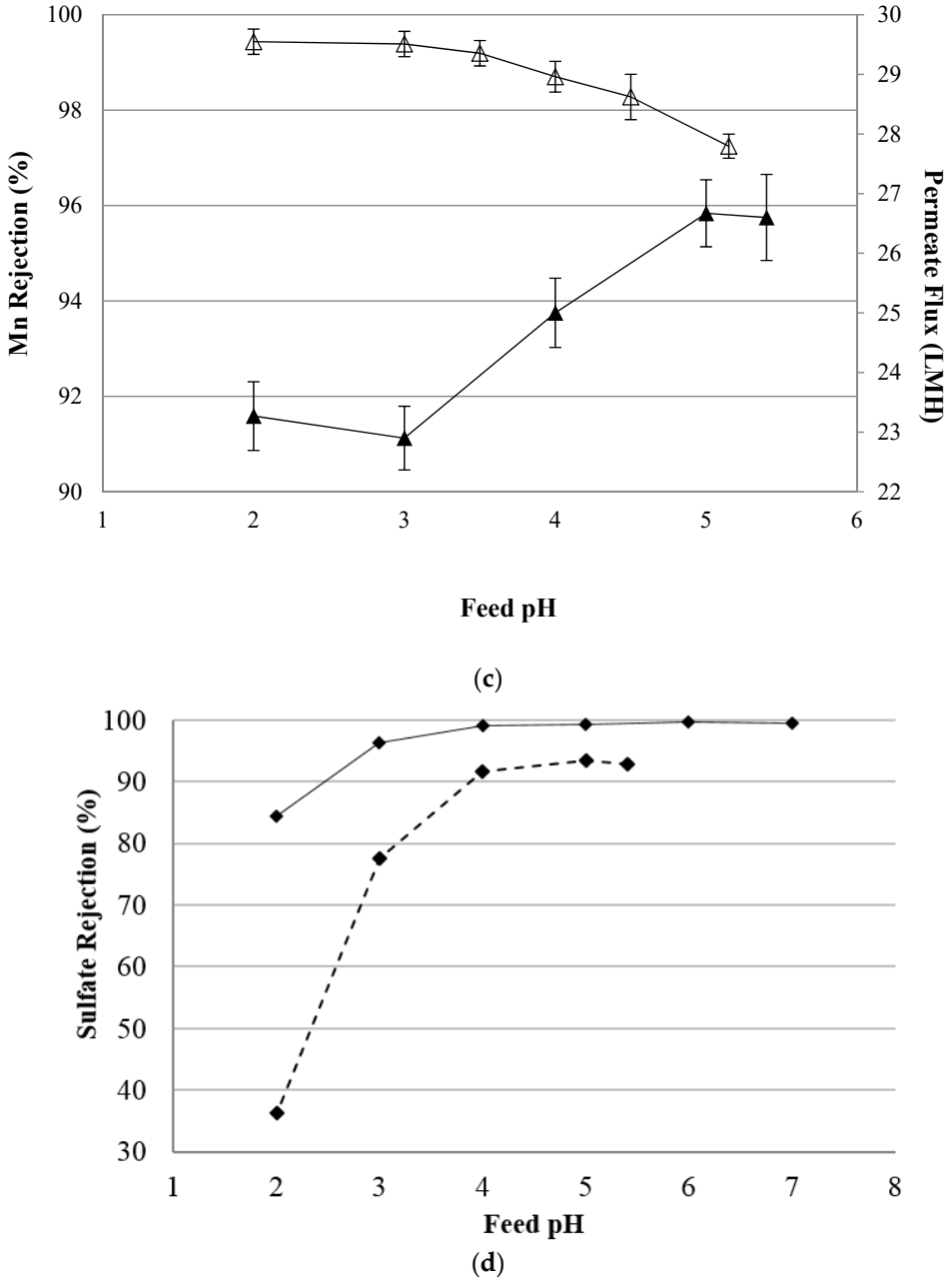

Figure 3. (**a**) Effect of feed pH on magnesium rejection (open symbol) and permeate flux (closed symbol). (Experimental conditions: $MgSO_4$ = 4000 mg/L, feed pressure = 10 bar, T = 25 °C). (**b**) Effect of feed pH on copper rejection (open symbol) and permeate flux (closed symbol) (Experimental conditions: $CuSO_4$ = 100 mg/L, feed pressure = 10 bar, T = 25 °C). (**c**) Effect of feed pH on apparent manganese rejection (open symbol) and permeate flux (closed symbol). (Experimental conditions: $Mn(NO_3)_2$ = 165 mg/L, feed pressure = 10 bar, T = 25 °C). (**d**) Effect of feed pH on apparent sulfate rejection. Feed solution containing 4000 mg/L $MgSO_4$ (full line) and 100 mg/L $CuSO_4$ (dotted line). (Experimental conditions: feed pressure = 10 bar, T = 25 °C).

As can be seen, the rejection of Mg^{2+} ions remained relatively constant (above 99.5%) throughout the investigated pH range, except for a slight dip at pH 5. This may be due to the proximity of this pH value to the membrane IEP, where a minimum ion rejection is to be expected [24,25]. The permeate flux, on the other hand, was higher as the pH value increased. This is contributed by the fact that the membrane became more negatively charged with increasing pH value as can be seen in Figure 2, resulting in a higher hydrophilicity [26–29]. As reported in the literature, dissociating groups in the

polymer skin layer can make the surface more hydrophilic and looser, when charges of the polymer chains start to repel each other at elevated pH [17].

As copper is one of the most commonly found elements in AMD, copper rejection was determined in a single salt rejection experiment, and the data obtained are presented in Figure 3b. It was found that Cu rejection increased slightly with increasing pH, with the lowest rejection of 98.6% at pH = 2 and the highest rejection of 99.1% at pH = 5.4. However, these rejection values can be interpreted as relatively constant after accounting for the standard deviation. For polyamide-based TFC membranes such as Desal DK and NF 270, a trend where the rejection of Cu ions increased with decreasing pH was reported [30,31]. This was due to electrostatic repulsion from the increasing positive charge. Consequently, the rejection of Cu in Membrane A was less dependent on the membrane charge as compared to commercial polyamide-based membranes for Cu rejection (see Figure 3b).

In terms of manganese rejection, Membrane A maintained relatively high values (above 97%) for the investigated pH range of 2 to 5 (Figure 3c). This can be explained by the increasing retention of positively charged manganese cations with respect to decreasing pH. Specific adsorption of Mn^{2+} cations could be expected to shift the IEP to a higher pH value due to the shielding of the negative membrane charge. As the pH decreased, a stronger electrostatic repulsion between Mn^{2+} and positive membrane charges occurred. Al Rashdi et al. [31] observed similar rejection values using NF270 where rejection was at a maximum of 90% at pH 1.5. However, the rejection of NF270 dropped rapidly to 20% near the membrane's IEP value. This shows that Membrane A produces more consistent and stable rejection results compared to NF270, which might be also associated with its denser polymeric structure and, therefore, the stronger contribution of steric (size-exclusion) compared to charge-related effects.

Sulfate rejection was determined in two different single salt solutions: 4000 mg/L magnesium sulfate and 100 mg/L copper (II) sulfate. It might be expected that in these solutions, due to complex co-adsorption of both the cations and the anions on the membrane surface, the IEP remains the same, but the overall surface charge becomes lower. As seen in Figure 3d, the rejection of sulfate in both solutions was relatively constant above the membrane IEP. This shows that the rejection of salt was governed mainly by the electrostatic repulsion of sulfate (SO_4^{2-}) and the negatively charged membrane.

Below the IEP, a sharp drop in sulfate rejection was observed, most remarkably at pH 2, which is close to the pKa value of sulfate (pKa = 1.92). This could be attributed to the increase in bisulfate (HSO_4^-) concentration in the feed solution due to chemical speciation of sulfate at lower pH values, which could trigger the Donnan effect [32]; at pH 2, sulfate ions are present as SO_4^{2-} and HSO_4^- with a ratio of ca. 10% and 50%, respectively [33].

The co-ion Mg^{2+} was rejected at a greater extent than H^+ due to its higher valence charge. Therefore, SO_4^{2-} anion remained with Mg^{2+} cation to maintain the overall electroneutrality on the feed side. At the same time, the monovalent HSO_4^- ions coupled with H^+ ions present in the solution, passing through the membrane to the permeate side, thus resulting in a lower permeate pH. The latter is also favored by the significantly higher concentration of very mobile protons (a "conductivity jump") at a feed pH lower than 3, which can lead to protons permeation (together with Cl^-) across the membrane. The overall membrane surface charge is also more shielded under such conditions.

As a result of the permeation of HSO_4^-, the overall sulfate rejection significantly decreased at pH values below the membrane IEP. This phenomenon was also observed by Visser et al. [34] and Mullett et al. [14], where sulfate rejection in a mixed system decreased drastically at pH 2 and 3. The fall in sulfate rejection at low pH (36.3% at pH = 2) was more drastic for the $CuSO_4$ experiment compared to the $MgSO_4$ experiment. The explanation for this phenomenon is that the higher permeation of SO_4^{2-} ions in the $CuSO_4$ solution can be attributed to the reduced effect of membrane charge shielding due to the lower salt concentration (100 mg/L of $CuSO_4$, in comparison to 4000 mg/L of $MgSO_4$).

4.3. NF Performance in Mixed-Salt Solutions

Due to the complexity of real acid mine drainage solutions, assessing the membrane performance during AMD filtration is precarious. The complexities arise from the interaction between the membrane

surface and the ions in the bulk solution. In addition, the solution chemistry of the bulk solution may change the membrane properties, resulting in different performance as previously tested in single salt solutions. In order to better understand how the membrane behaves in a more complex solution, three different mixed salt solutions were prepared as shown in Table 2.

Chloride rejection (Figure 4) was obtained by performing a charge balance (∑ Charge of Cations = ∑ Charge of Anions) on both the feed and permeate side while taking into account the speciation of sulfate at pH lower than 3. At pH 2, it can be expected that the co-ions, H^+, coupled with either Cl^- or SO_4^{2-} counter ions to pass through the membrane as HCl and H_2SO_4, while Na^+ remains in the feed side. At relatively low concentrations of H^+, within the range of pH 5 to 7, Na^+ rejection (Figure 4) remained high and almost constant.

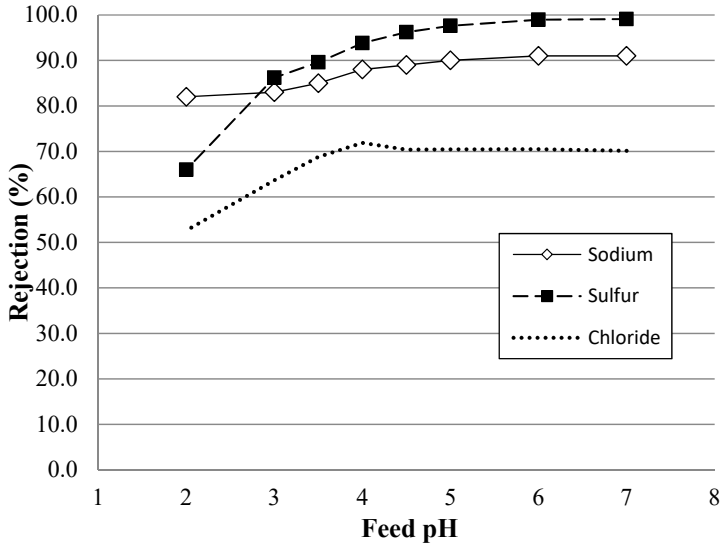

Figure 4. Apparent sulfur rejection (dashed line) sodium rejection (full line) and chloride rejection (dotted line) as a function of pH for Na_2SO_4 and NaCl mixed salt solution. Experimental conditions: feed pressure = 10 bar, T = 25 °C. Concentrations of Na_2SO_4 and NaCl = 2000 mg/L and 700 mg/L, respectively.

A slight decrease in permeate pH was observed for a feed range of pH 5 to 7 (Figure 5). This may be due to the increased rejection of the trace amounts of OH^- brought about by the more negatively charged membrane at higher pH.

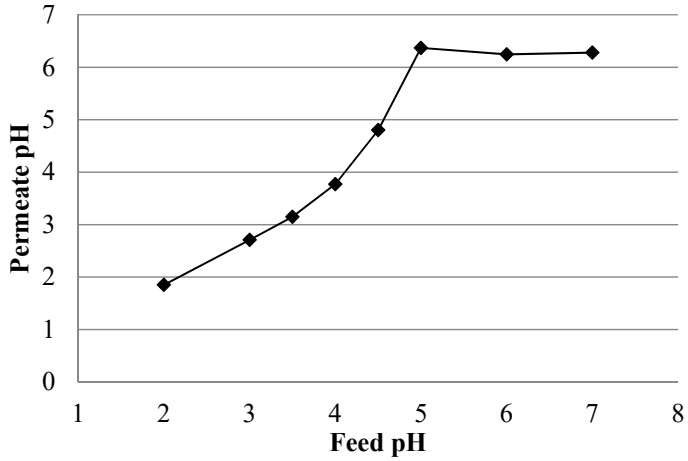

Figure 5. Permeate pH as a function of feed pH for Na_2SO_4 and NaCl mixed salt solution.

For single salt sodium silicate solution at pH 7, uncharged H_2SiO_3 was the dominant silicate species in the solution and $HSiO_3^-$ was present in trace amounts. Size exclusion was the main rejection mechanism for silicate, thus accounting for the low rejection value of 52.42% (Figure 6). When magnesium sulfate was introduced into the single salt sodium silicate solution, silicate rejection fell further to 38.56%. This was due to the effect of charge shielding by Mg^{2+} on the negatively charged membrane. $HSiO_3^-$ was rejected to a lesser extent. Similarly, magnesium sulfate rejection falls in a mixed salt solution due to the shielding effect of the negatively charged membrane by Na^+ ions.

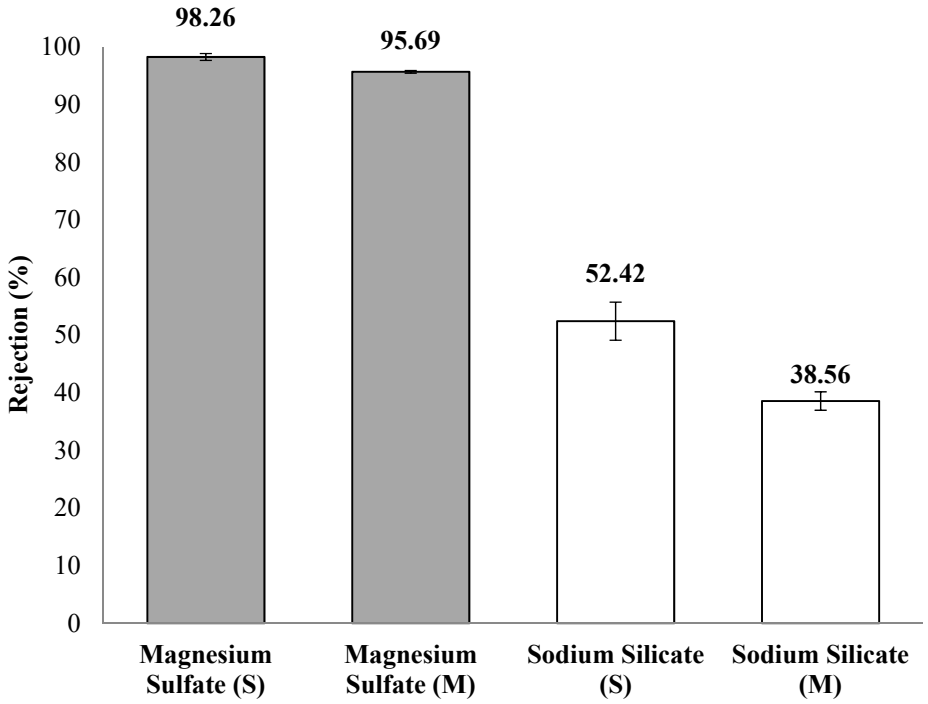

Figure 6. Magnesium sulfate (grey) and sodium nitrate apparent rejection (white) in the single (S) and mixed (M) solutions. Experimental conditions: feed pressure = 10 bar, 25 °C.

At pH 7, Membrane A is negatively charged. At this pH value, rejection of sulfate is greater than the chloride due to stronger electrostatic repulsion (higher valency in SO_4^{2-} vs. Cl^-), thus resulting in a system behavior influenced by the Donnan effect related phenomenon, occurring due to preferential rejection of divalent compared to monovalent ions. Passage of Cl^- is more prominent at higher salt concentrations due to the screening effect brought about by increasing Na^+ concentrations. The presence of Na^+ shields the negative charge on the membrane surface, thus causing a decreased Cl^- rejection. Due to its higher valency and larger size, the rejection of sulfate was high for all tested concentrations and was less dependent on the membrane charge (see Figure 7).

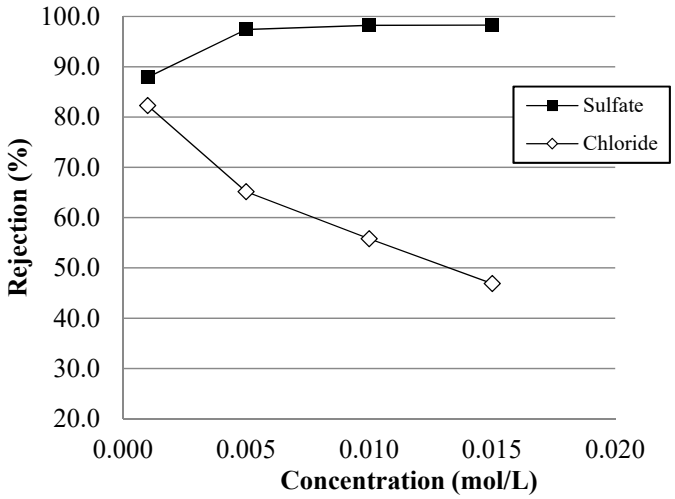

Figure 7. Effect of salt concentration on apparent sulfate and chloride rejection. Experimental conditions: feed pressure = 10 bar, 25 °C.

4.4. Simulated AMD Solutions

In the simulated AMD solution, rejection minima were observed at pH 4 (Figure 8). This value is close to the IEP of Membrane A for which the net charge of the membrane approaches zero. At the IEP, size exclusion is the remaining rejection mechanism, therefore, an increased passage of metal ions is registered. The observed rejection minimum (at pH = 4.0) was lower than the IEP obtained from the zeta potential measurement at membrane IEP of pH 4.5–4.7. The observed shift of minimal rejection can be attributed to the fact that the IEP measurements are dependent on the solution chemistry that the membrane is exposed to. Thus, the observed difference in the IEP for the model AMD solution may be due to the adsorption of divalent sulfate anions present in the solution onto the membrane.

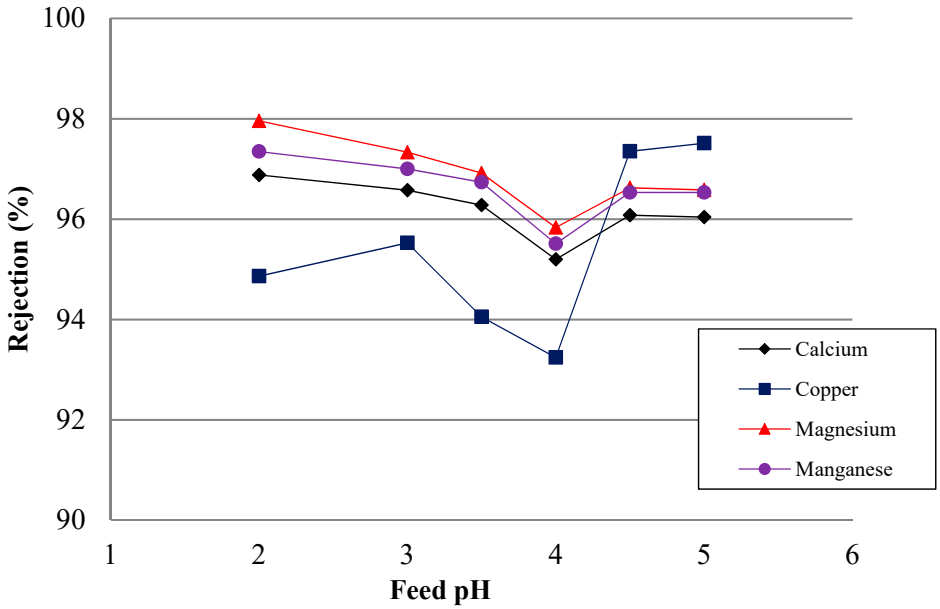

Figure 8. Apparent metal species rejection as a function of feed pH.

With the exception of copper, metal ions rejection increased with decreasing pH due to stronger electrostatic repulsion brought about by a more positively charged membrane. An opposite trend was observed for copper, for which rejection increases with increasing pH. This is possibly due to the appearance of a negatively charged copper complexes, such as $Cu(OH)_{3-}$, which become increasingly

rejected by the more negatively charged membrane with increasing pH. The permeate flux (shown in Figure 9) remains relatively constant throughout the tested pH range. The permeate pH values were lower than the feed pH ones, especially for feed pH lower than 4 as H^+ couples with anions and passes through the membrane.

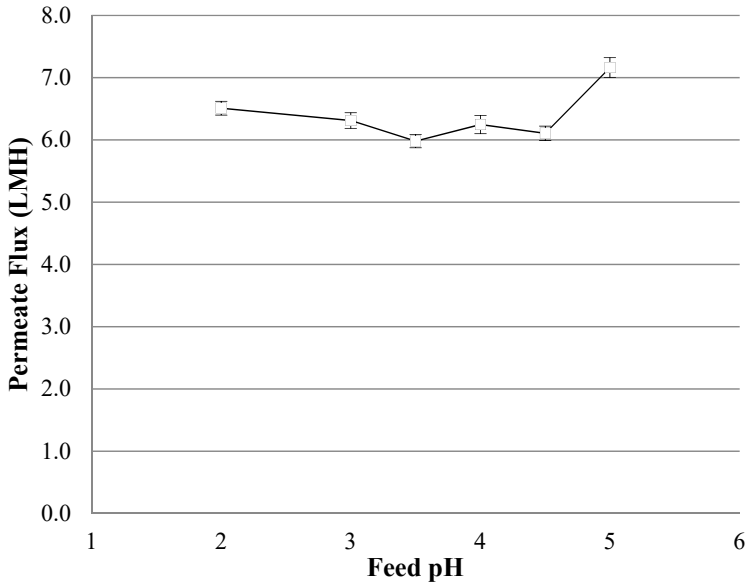

Figure 9. AMD permeate flux as a function of feed pH.

Sodium rejection was lower than that for the larger size divalent cations. In general, sodium rejection increases with increasing solution pH (a more negatively charged membrane). As seen can be in Figure 10, at higher pH, sodium rejection displays a higher rejection value as accompanying divalent anions (SO_4^{2-}) are highly rejected. However, sodium rejection was lower than expected. This may possibly be due to the permeation of sodium cations with monovalent anions (nitrate and chloride). The anions rejection increases with increasing pH due to a stronger electrostatic repulsion from the negative membrane. Due to their monovalent nature and smaller size, nitrate and chloride expectedly showed lower rejection values than those for sulfate.

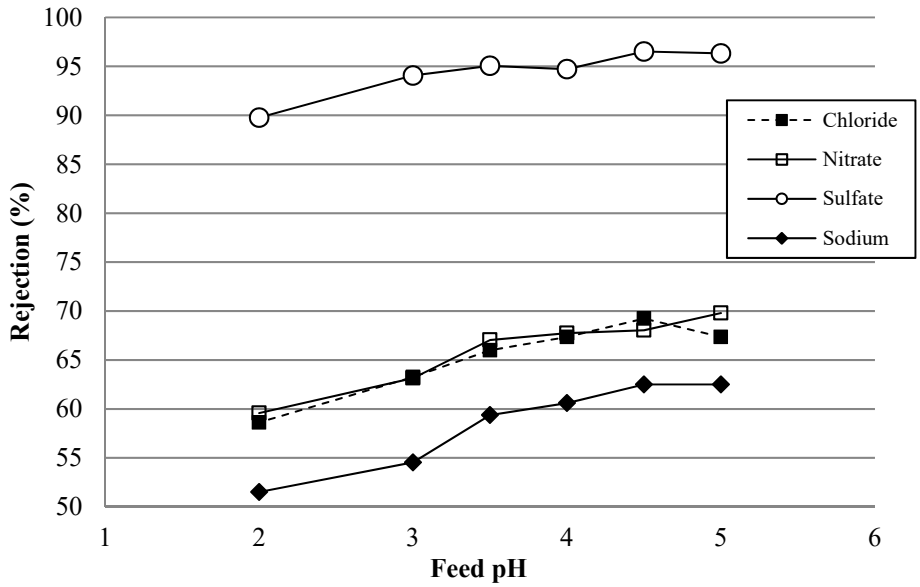

Figure 10. Apparent species rejection as a function of feed pH.

While not substituting the necessity of performing validation tests using real acid mine drainage water in a defined case, the results obtained with the simulated AMD solutions can be used as a fast and preliminary evaluation tool of expected performance of the membrane in nanofiltration of real water with a known ionic composition and pH.

5. Conclusions

Rejection of ions in single salt solutions were found to be pH-dependent. Owing to their large size, all-metal cations (Mg, Cu, and Mn) were highly rejected (97% and above) within the tested pH range. Below the membrane IEP, cation rejection increased slightly as a result of stronger electrostatic repulsion between the cations (co-ions) and the positively-charged membrane (e.g., the rejection increased from 97% at pH 5 to 99% at pH 2).

The speciation of divalent sulfate to monovalent bisulfate at pH 3 and below accounted for the sharp fall in overall sulfate rejection. Notably, sulfate rejection fell from 99% at pH 4 to 84% at pH 2. The effect of sulfate speciation on rejection was more pronounced under conditions of a weaker membrane charge shielding at lower ionic strength.

In general, the rejection of ions in mixed salt solutions were lower compared to the rejection of single salt solutions mainly due to the effect of membrane charge shielding at increased ionic strength. For a sodium silicate solution, silicate rejection fell from 52% to 38% when magnesium sulfate was added to the feed solution. Donnan effects were more prominent at higher salt concentrations. Rejection of monovalent co-ion (chloride) decreased with increasing concentration of an accompanying divalent co-ion (sulfate).

For the model AMD solution, a minimal rejection was observed at pH 4. The shift in IEP from 4.5 to 4.0 was most probably due to divalent anion adsorption at the relatively higher ionic strength of the solution. Copper showed an interesting trend of increasing rejection with increasing pH most probably attributed to the formation of a negatively charged complex formation, while other metal cations displayed rejection values in the opposite direction.

Author Contributions: Conceptualization, K.L.Z. and S.V.; methodology, K.L.Z. and S.V.; validation, Y.W.S., K.L.Z. and S.V.; formal analysis, Y.W.S.; investigation, Y.W.S; resources, K.L.Z.; data curation, Y.W.S.; writing—original draft preparation, Y.W.S; writing—review and editing, S.V and K.L.Z.; visualization, Y.W.S.; supervision, K.L.Z. and S.V.; project administration, K.L.Z.; funding acquisition, K.L.Z. All authors have read and agreed to the published version of the manuscript.

Funding: The authors would like to thank LANXESS-IAB Ionenaustauscher GmbH (Bitterfeld, Germany) for financial support. Ye Wee Siew acknowledges his scholarship grant provided by the European Commission—Education, Audiovisual, and Culture Executive Agency (EACEA), under the program: Erasmus Mundus Master in Membrane Engineering–EM3E (FPA No 2011e0168, Ed. I, http://em3e-4sw.eu).

Conflicts of Interest: The authors declare no conflict of interest.

Appendix A. Supporting Information

Concentration Polarization

Concentration polarization was deliberately provoked in the coupon tester by lowering the cross flow rate from 4.0 L/min to 0.5 L/min at two different conditions (Table A1). Apparent rejection (Equation (5)) and salt passage were the membrane performance parameters evaluated in these experiments. Salt passage is defined as the ratio of the concentration of salt on the permeate relative to the feed side as:

$$SP = \frac{C_p}{C_f} = 1 - R. \quad \text{(A1)}$$

Feed and permeate concentrations were determined using conductivity vs. concentration calibration curves.

For both experiments, the salt passage (Figures A1 and A2) increased slightly when the cross flow rate was decreased from 2.0 L/min to 0.5 L/min. Above 2.0 L/min, salt passage remained relatively constant for both cases. This shows that concentration polarization occurs only at a low cross flow rate due to decreased tangential shear stress on the membrane surface. Thus, concentration polarization effects in the coupon tester for this study can be assumed to be negligible as they were all performed at cross flow rate of 4 L/min.

Table A1. Concentration polarization experiments operating conditions.

Temperature (°C)	Feed Concentration (mg/L)	Feed Pressure (Bar)
25 ± 0.5	2000 ± 100 of $MgSO_4$ 8000 ± 200 of $MgSO_4$	10 ± 0.1 25 ± 0.1

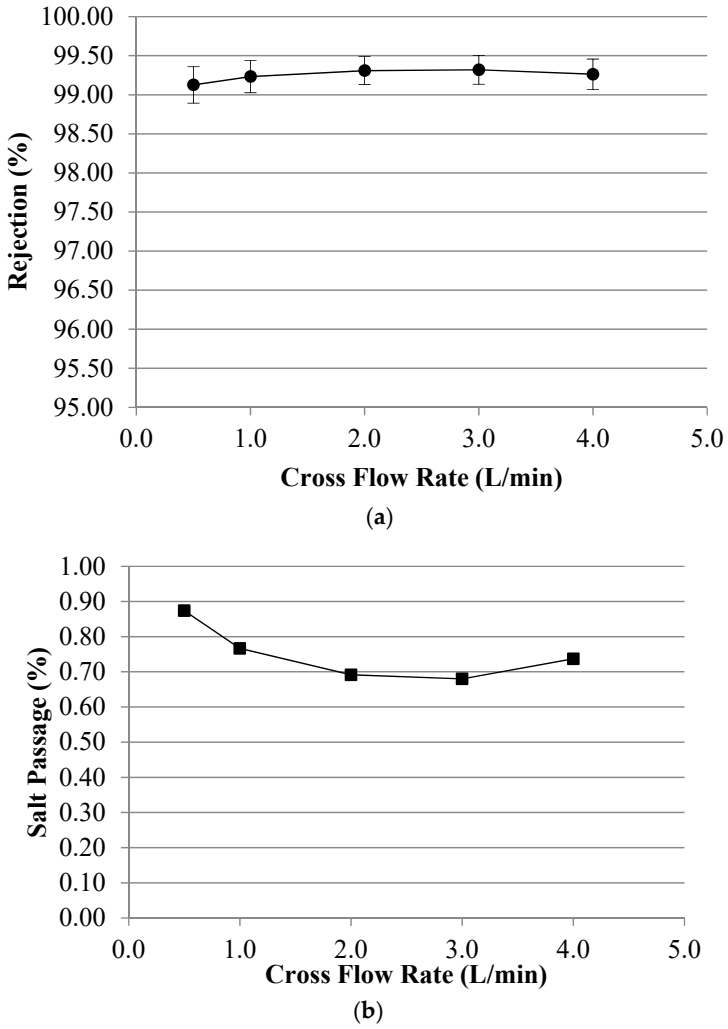

Figure A1. (**a**) Graph of rejection as a function of the cross flow rate (Operating Conditions: 2000 mg/L $MgSO_4$, pH 7, 25 °C, and 10 bar). (**b**) Graph of salt passage as a function of the cross flow rate (Operating Conditions: 2000 mg/L MgSO4, pH 7, 25 °C, and 10 bar).

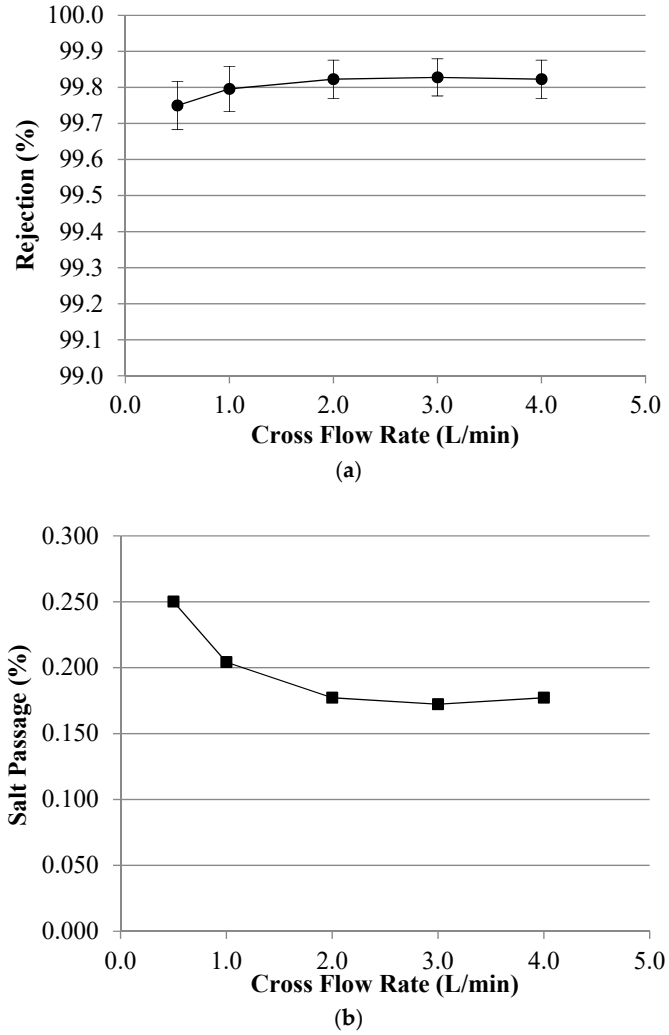

Figure A2. (**a**) Graph of rejection as a function of the cross flow rate (Operating Conditions: 8000 mg/L $MgSO_4$, pH 7, 25 °C, and 25 bar). (**b**) Graph of salt passage as a function of cross flow rate (Operating Conditions: 8000 mg/L $MgSO_4$, pH 7, 25 °C, and 25 bar).

Appendix B. Symbols and Nomenclature

Symbols	Parameter	Units
R_{app}	Apparent rejection	%
c_p	Concentration of solute on the permeate side	$mg{\cdot}L^{-1}$
c_f	Concentration of solute on the feed side	$mg{\cdot}L^{-1}$
Π	Osmotic pressure	bar
i	Dimensionless van't Hoff factor	-
M	Molarity	$mol{\cdot}L^{-1}$
R	Ideal gas constant	L bar K^{-1} mol^{-1}
T	Temperature	K
t	Time	h
$\Delta\Pi$	Osmotic pressure difference	bar
Πf	Feed osmotic pressure	bar
Πp	Permeate osmotic pressure	bar
J_v	Permeate flux	$L{\cdot}m^{-2}{\cdot}h^{-1}$
A	Water permeability coefficient	$L{\cdot}m^{-2}{\cdot}h^{-1}$ bar^{-1}
ΔP	Applied pressure	bar
V_p	Permeate volume	m^3
A_m	Membrane area	m^2

References

1. Akcil, A.; Koldas, S. Acid Mine Drainage (AMD): Causes, treatment and case studies. *J. Clean. Prod.* **2006**, *14*, 1139–1145. [CrossRef]
2. Simate, G.S.; Ndlovu, S. Acid mine drainage: Challenges and opportunities. *J. Environ. Chem. Eng.* **2014**, *2*, 1785–1803.
3. Johnson, D.B.; Hallberg, K.B. Acid mine drainage remediation options: A review. *Sci. Total Environ.* **2005**, *338*, 3–14. [CrossRef]
4. Gitari, M.W.; Petrik, L.F.; Etchebers, O.; Key, D.L.; Iwuoha, E.; Okujeni, C. Treatment of Acid Mine Drainage with Fly Ash: Removal of Major Contaminants and Trace Elements. *J. Environ. Sci. Heal. Part A* **2006**, *41*, 1729–1747. [CrossRef]
5. Younger, P.L.; Banwart, S.A.; Hedin, R.S. *Mine Water: Hydrology, Pollution, Remediation*; Kluwer Academic Publishers: Dordrecht, The Netherlands, 2002; Volume 9.
6. Al-Zoubi, H.; Rieger, A.; Steinberger, P.; Pelz, W.; Haseneder, R.; Härtel, G. Optimization Study for Treatment of Acid Mine Drainage Using Membrane Technology. *Sep. Sci. Technol.* **2010**, *45*, 2004–2016. [CrossRef]
7. Watten, B.J.; Sibrell, P.L.; Schwartz, M.F. Acid neutralization within limestone sand reactors receiving coal mine drainage. *Environ. Pollut.* **2005**, *137*, 295–304. [CrossRef] [PubMed]
8. Al-Zoubi, H.; Rieger, A.; Steinberger, P.; Pelz, W.; Haseneder, R.; Härtel, G. Nanofiltration of Acid Mine Drainage. *Desalin. Water Treat.* **2010**, *21*, 148–161. [CrossRef]
9. Sheoran, A.; Sheoran, V.; Choudhary, R. Bioremediation of acid-rock drainage by sulphate-reducing prokaryotes: A review. *Miner. Eng.* **2010**, *23*, 1073–1100. [CrossRef]
10. Dąbrowski, A.; Hubicki, Z.; Podkościelny, P.; Robens, E. Selective removal of the heavy metal ions from waters and industrial wastewaters by ion-exchange method. *Chemosphere* **2004**, *56*, 91–106. [CrossRef]
11. Nodwell, M.; Kratochvil, D. Sulphide Precipitation and Ion Exchange Technologies to Treat Acid Mine Drainage. In Proceedings of the 9th International Conference on Acid Rock Drainage, Ottawa, ON, Canada, 20–26 May 2012.
12. López, J.; Reig, M.; Gibert, O.; Cortina, J. Integration of nanofiltration membranes in recovery options of rare earth elements from acidic mine waters. *J. Clean. Prod.* **2019**, *210*, 1249–1260. [CrossRef]
13. Rieger, A.; Steinberger, P.; Pelz, W.; Haseneder, R.; Härtel, G. Mine water treatment by membrane filtration processes-Experimental investigations on applicability. *Desalin. Water Treat.* **2009**, *6*, 54–60. [CrossRef]
14. Mullett, M.; Fornarelli, R.; Ralph, D. Nanofiltration of Mine Water: Impact of Feed pH and Membrane Charge on Resource Recovery and Water Discharge. *Membranes* **2014**, *4*, 163–180. [CrossRef] [PubMed]
15. Hagmeyer, G.; Gimbel, R. Modelling the rejection of nanofiltration membranes using zeta potential measurements. *Sep. Purif. Technol.* **1999**, *15*, 19–30. [CrossRef]
16. Ferreira Esmi, C.; Schrive, L.; Barre, Y.; Palmeri, J.; Deratani, A. Using nanofiltration in a zero-rejection process: The removal of Ni 2+ and Co 2+ from salty wastewater. *Desalin. Water Treat.* **2013**, *51*, 476–484. [CrossRef]
17. Mänttäri, M.; Pihlajamäki, A.; Nyström, M. Effect of pH on hydrophilicity and charge and their effect on the filtration efficiency of NF membranes at different pH. *J. Membr. Sci.* **2006**, *280*, 311–320. [CrossRef]
18. Tang, B.; Huo, Z.; Wu, P. Study on a novel polyester composite nanofiltration membrane by interfacial polymerization of triethanolamine (TEOA) and trimesoyl chloride (TMC). *J. Membr. Sci.* **2008**, *320*, 198–205. [CrossRef]
19. Lianchao, L.; Baoguo, W.; Huimin, T.; Tianlu, C.; Jiping, X. A novel nanofiltration membrane prepared with PAMAM and TMC by in situ interfacial polymerization on PEK-C ultrafiltration membrane. *J. Membr. Sci.* **2006**, *269*, 84–93. [CrossRef]
20. Werner, C.; Körber, H.; Zimmermann, R.; Dukhin, S.; Jacobasch, H.-J. Extended electrokinetic characterization of flat solid surfaces. *J. Colloid Interface Sci.* **1998**, *208*, 329–436. [CrossRef]
21. Zimmermann, R.; Dukhin, S.; Werner, C. Electrokinetic measurements reveal interfacial charge at polymer films caused by simple electrolyte ions. *J. Phys. Chem. B* **2001**, *105*, 8544–8549. [CrossRef]
22. Bellmann, C.; Klinger, C.; Opfermann, A.; Böhme, F.; Adler, H.-J.P. Evaluation of surface modification by electrokinetic measurements. *Prog. Org. Coat.* **2002**, *44*, 93–98. [CrossRef]
23. Cadotte, J.; Forester, R.; Kim, M.; Peterson, R.; Stocker, T. Nanofiltration membranes broaden the use of membrane separation technology. *Desalination* **1988**, *70*, 77–88. [CrossRef]

24. Childress, A.E.; Elimelech, M. Relating nanofiltration membrane performance to membrane charge (electrokinetik) characteristics. *Environ. Sci. Technol.* **2000**, *34*, 3710–3716. [CrossRef]
25. Luo, J.; Wan, Y. Effects of pH and salt on nanofiltration—A critical review. *J. Membr. Sci.* **2013**, *438*, 18–28. [CrossRef]
26. Childress, A.E.; Elimelech, M. Effect of solution chemistry on the surface charge of polymeric reverse osmosis and nanofiltration membranes. *J. Membr. Sci.* **1996**, *119*, 253–268. [CrossRef]
27. Hoang, T.; Stevens, G.; Kentish, S. The effect of feed pH on the performance of a reverse osmosis membrane. *Desalination* **2010**, *261*, 99–103. [CrossRef]
28. Szymczyk, A.; Fievet, P.; Bandini, S. On the amphoteric behavior of Desal DK nanofiltration membranes at low salt concentrations. *J. Membr. Sci.* **2010**, *355*, 60–68. [CrossRef]
29. Lopez, J.; Reig, M.; Gibert, O.; Valderrama, C.; Cortina, J. Evaluation of NF membranes as treatment technology of acid mine drainage: Metals and sulfate removal. *Desalination* **2018**, *440*, 122–134. [CrossRef]
30. Ku, Y.; Chen, S.; Wang, W. Effect of solution composition on the removal of copper ions by nanofiltration. *Sep. Purif. Technol.* **2005**, *43*, 135–142. [CrossRef]
31. Al-Rashdi, B.; Johnson, D.; Hilal, N. Removal of heavy metal ions by nanofiltration. *Desalination* **2013**, *315*, 2–17. [CrossRef]
32. Donnan, F.G. Theory of membrane equilibria and membrane potentials in the presence of non-dialysing electrolytes. A contribution to physical-chemical physiology. *J. Membr. Sci.* **1995**, *100*, 45–55. [CrossRef]
33. Mazlan, J.; Myneni, S.C.B. Speciation of iron and sulfate in acid waters: Aqueous clusters to mineral precipitates. *Environ. Sci. Technol.* **2005**, *39*, 188–194. [CrossRef] [PubMed]
34. Visser, T.; Modise, S.; Krieg, H.; Keizer, K. The removal of acid sulphate pollution by nanofiltration. *Desalination* **2001**, *140*, 79–86. [CrossRef]